Cancer Research

Lactic Acid Accumulation in the Tumor Microenvironment Suppresses ^{18}F-FDG Uptake

Silvan Türkcan[1], Louise Kiru[1], Dominik J. Naczynski[1], Laura S. Sasportas[2], and Guillem Pratx[1]

Abstract

The process by which tumor cells take up 2-[^{18}F]fluoro-2-deoxy-D-glucose (FDG) is heterogeneous and influenced by a multitude of factors. In mouse tumor grafts, the core of the tumor often presents lower FDG uptake than the periphery. Whether this pattern is caused by the intrinsic avidity of individual cells for FDG, the density of viable cells in the tumor, or the perfusion of the radiotracer remains unknown. In this study, we used radioluminescence microscopy to measure FDG uptake in single cells isolated from the core and periphery of the tumor and found that differences in FDG uptake persist on the level of single cells. Single cells from the core of 4T1 and MDA-MB-231 tumors grafts took up 26% to 84% less FDG than those from the periphery. These differences were observed in mice with large tumors (>8 mm diameter) but not in those with smaller tumors. To explain the origin of these differences, we examined the influence of three microenvironmental factors on FDG uptake. Hypoxia was ruled out as a possible explanation because its presence in the core would increase and not decrease FDG uptake. Higher cell proliferation in the periphery was consistent with higher FDG uptake, but there was no evidence of a causal relationship. Finally, lactate was higher in the core of the tumor, and it suppressed FDG uptake in a dose-dependent fashion. We therefore conclude that lactic acidosis—the combination of lactate ion buildup and acidic pH—can increase the heterogeneity of FDG uptake in MDA-MB-231 and 4T1 tumor grafts.

Significance: Analysis of single cells from heterogeneous tumors reveals the role played by the tumor microenvironment, lactic acidosis in particular, on the uptake by tumor cells of ^{18}F-FDG, a PET imaging agent.

Introduction

Positron emission tomography (PET) has become an indispensable tool for cancer diagnosing, staging, and monitoring. The glucose analog 2-[^{18}F]fluoro-2-deoxy-D-glucose (FDG) is commonly used radiotracer to assess the metabolic activity of cancer cells (1). FDG-PET can reliably identify and characterize tumors owing to their increased demand for glucose compared with normal tissues (2). This avidity of tumor cells for glucose depends on a range of biological factors, and, therefore, interpreting FDG-PET images is prone to errors in distinguishing between malignant and benign lesions, and in predicting tumor response to therapy (3). In addition, the low resolution of PET and the resulting partial volume effect can obscure the impact of cell-type heterogeneity on the calculation of the standardized uptake value, such as when activated leukocytes infiltrate the tumor. Therefore, it is important to understand what biological factors drive FDG uptake measured in clinical scans.

Challenges in interpreting PET scans are exacerbated by the heterogeneous architecture of the tumor (4, 5) and its microenvironment (6–9). Microenvironmental factors within a solid tumor that influence cell biology include vasculature, lymphatics, infiltration of immune cells, interstitial fluid pressure, hypoxia, and acidosis. Through the expression of genes such as HIF1A (10–12), these factors modulate tumor cell metabolism by altering the expression level and activity of glucose transporters (primarily GLUT-1 and GLUT-3) and hexokinase enzymes. Previous experiments that measured bulk FDG uptake in cell lines have shown these proteins to be the main predictors of FDG uptake in cells (13–16) and tumor tissue (17, 18), and FDG uptake is directly related to the metabolic flux of glucose through glycolysis. Cell proliferation and cell cycle have also been shown to influence FDG uptake at the tissue level (15).

In heterogeneous tumor tissues, studies combining autoradiography with tissue staining (Hoechst 33342 for perfusion, pimonidazole for hypoxia, and bromodeoxyuridine or Ki-67 for proliferation) generally show the following trends: FDG uptake tends to be lower in oxygenated, well-perfused, and proliferating areas, and higher in hypoxic areas (11, 12, 19, 20). However, these studies were based on autoradiography of tissue sections, which cannot separate cell-intrinsic biological factors from tracer perfusion and density of viable cells. Each pixel in a storage-phosphor autoradiography image has a spatial resolution of approximately 100 μm and thus combines signals from >100 cells. With PET, the spatial resolution is even more limited (4–8 mm for clinical scanners), and the smallest resolvable structure corresponds to >10^8 cells. These imaging techniques cannot be used to determine whether differences in FDG uptake are due to intrinsic metabolic properties, the perfusion of the tracer, or to the density of viable tumor cells.

[1]Department of Radiation Oncology, Stanford University School of Medicine, Stanford, California. [2]Department of Radiology, Stanford University School of Medicine, Stanford, California.

Note: Supplementary data for this article are available at Cancer Research Online (http://cancerres.aacrjournals.org/).

S. Türkcan and L. Kiru contributed equally to this article.

Corresponding Author: Guillem Pratx, Stanford University, 300 Pasteur Dr, Grant S277, Stanford, CA 94305. Phone: 650-724-9829; E-mail: pratx@stanford.edu

doi: 10.1158/0008-5472.CAN-17-0492

To better understand the heterogeneity of radiotracer uptake and its relationship to other biological factors, we recently developed radioluminescence microscopy (RLM), a technique that can image radiotracer uptake at the single-cell level, inside a fluorescence microscope (21, 22). Here, we applied RLM imaging to determine how the properties of the tumor microenvironment affect FDG uptake in single cells dissociated from tumor grafts.

We focused this investigation on a pattern of tumor heterogeneity, commonly observed in tumor grafts, where the periphery of the tumor presents higher FDG uptake than the core. We surgically separated tumors into these two components and further dissociated each component into a single-cell suspension. We then used RLM to quantify FDG uptake in single cancer cells. Because *in vitro* cells are exposed to the same amount of FDG, differences in mean FDG uptake between core and periphery reflect intrinsic metabolism and not tissue perfusion or viable cell density. Finally, we determined the effect of several microenvironment factors (hypoxia, low nutrient availability, and high lactate levels) on FDG uptake by reproducing these conditions *in vitro* in the same cell lines. By combining the data obtained from *in vitro* and *in vivo* studies, we identified lactic acidosis as an important modulator of FDG uptake in tumors.

Materials and Methods

Cell culture

Luciferase-expressing MDA-MB-231 human breast cancer cells were obtained from Cell Biolabs, Inc. in April 2016 (cat. number AKR 231) and passaged no more than 8 times. The 4T1 mouse mammary cancer cell line was purchased from the ATCC (cat. number CRL-2539) in 2010 and cultured without exceeding passage 20. This cell line was previously transfected with a lentiviral construct containing a bifusion reporter of enhanced green fluorescent protein (eGFP) and firefly luciferase-2 (23). In addition, these cells were tested in house for *Mycoplasma* using Lonza MycoAlert Detection Kit (cat. number LT07-118). The cell lines were not further authenticated. For most experiments, cells were grown at 37°C and 5% CO_2 in DMEM medium supplemented with 10% FBS and 1% penicillin–streptomycin (Life Technologies). For experiments involving pH and lactic acid, we changed the culture medium to RPMI 1640 because the concentration of sodium bicarbonate buffer is comparable with that of human plasma (1.8–2.3 g/L). Although widely used for cell culture, DMEM is strongly buffered, with nearly twice as much (3.7 g/L) sodium bicarbonate as RPMI. Cells were trypsinized and counted before being plated for microscopy studies. For RLM imaging, glass-bottom imaging dishes (CellVis) were coated with 5 μg/mL human fibronectin (BD biosciences), and cells were plated 2 days prior to imaging.

Animal models

All animal studies were approved by the Stanford University Administrative Panel on Laboratory Animal Care under protocol #23007. Female Nu/Nu mice were purchased from Charles River Laboratories. Cancer cells (MDA-MB-231 or 4T1) were freshly harvested and suspended in matrigel/PBS (1:1). A 20 μL solution of matrigel containing 1×10^6 cells was injected subcutaneously into both flanks, and tumors were allowed to grow over 2 to 3 weeks.

MicroPET/CT imaging

Food was withheld from the mice 4 hours prior to imaging. After anesthetizing animals with 4% isoflurane gas, we intravenously administered a dose of 20 MBq FDG per animal. MicroPET-CT imaging was performed 30 minutes after injection using a Siemens Inveon PET-CT under anesthesia, with an acquisition time of 5 minutes and standard reconstruction.

Tissue dissociation

Tumors were harvested after euthanasia and rinsed in PBS, then surgically separated into two components, the periphery and the core. Both samples were minced with a scalpel and transferred into ice-cold Trypsin. Tumors and trypsin were brought to 37°C for 30 minutes while being vortexed. The solution was decanted through a 40 μm strainer to separate single cells and centrifuged. Cells were resuspended in growth media and plated on coverslips or cell culture flasks.

Autoradiography

Tumors were harvested posteuthanasia 60 minutes after FDG injection, after completion of the PET study. The tumor was embedded in optimal cutting temperature compound (Sakura Finetek), cooled to −20°C, sectioned into 10-μm-thin sections with a microtome, and transferred onto a glass coverslip. Autoradiography was performed on a standard storage-phosphor film (PerkinElmer) overnight.

RLM imaging

Prior to imaging, cells were fasted in glucose-free DMEM or RPMI medium supplemented with 10% FBS for 45 minutes at 37°C and 5% CO_2. Subsequently, FDG (20 MBq/mL) was introduced into the dish for uptake by cells for 45 minutes (37°C and 5% CO_2). The cells were then washed 3 times with DMEM medium supplemented with 10% FBS to remove residual FDG. Following these preparations, the cells were imaged using RLM (Supplementary Fig. S1A) using a $CdWO_4$ scintillator (1 cm × 1 cm × 0.5 mm, 2 sides polished, MTI Inc.). Images of individual ionization tracks were serially acquired using an EM-CCD (Hamamatsu ImageEM C9100-14) with maximum gain, 50–200 ms integration time, and 4 × 4 binning. The integration time was chosen to average about 10 decay events per frame. Reconstructed RLM images were obtained by our methodology called optical reconstruction of the beta-ionization track as previously described in detail (24). The methodology is summarized in the supporting material (Supplementary Fig. S1). Region-of-interest (ROI) analysis of single cells was performed on the reconstructed images by measuring the total number of counts inside circular ROIs placed manually on individual cells, using the corresponding brightfield and bioluminescence images as a reference.

Digital RT-PCR

RNA was isolated from cells using the mirVana miRNA isolation Kit (Life Technologies) per the manufacturer's protocol and converted to cDNA. The expression levels of 84 hypoxia-associated genes were determined with a RT 2 Profiler PCR Mouse Hypoxia Signaling Pathway Array (Qiagen) using RT-PCR with the SYBR Green-optimized primer (Qiagen) on a RT-PCR instrument (ABI OneStepPlus, Life Technologies). The expression levels were normalized using five housekeeping genes in the RT 2 Profiler PCR array and analyzed using the Qiagen software bundle.

Effect of chronic hypoxia on FDG uptake

MDA-MB-231 or 4T1 cells were seeded on 25 mL cell culture flasks (Corning Incorporated). The cells were placed in a 2% O_2 hypoxia chamber (Ruskinn Technology Limited) or a Forma

SteriCycle i160 CO_2 incubator (ThermoFisher Scientific), both running at 37°C and 5% CO_2 (normoxia). On day 6, the cells were plated on 35-mm imaging dishes (Ibidi) and placed back into the hypoxia chamber or CO_2 incubator. On the next day, cells were fasted in glucose-free DMEM medium supplemented with 10% bovine serum for 30 minutes. The cells were subsequently incubated with FDG (20 MBq/mL) for 30 minutes at 37°C under 5% CO_2 and washed 3 times with glucose-free DMEM medium supplemented with 10% bovine serum. RLM imaging was performed as previously described above.

5-Ethynyl-2′deoxyuridine fluorescence imaging

Cells were grown on microscopy coverslips with and without serum, and then incubated with 5-ethynyl-2′deoxyuridine (EdU) working solution from the Click-iT EdU Imaging Kit (Invitrogen). Following incorporation of EdU for 1 hour at 37°C, EdU detection is performed by labeling EdU with Alexa Fluor azide following the manufacturer's protocol. In addition, the nuclei were stained with Hoechst 33342 dye. Cells were subsequently imaged on a fluorescence microscope with GFP filter set to detect Alexa 488 EdU signal and a DAPI filter set to image the blue Hoechst dye. The number of nuclei and EdU-positive nuclei was estimated by thresholding the image and applying a particle detection algorithm in ImageJ.

Histology and quantification

MDA-MB-231 or 4T1 tumors were harvested and placed in 4% paraformaldehyde. The untrimmed tumors were embedded in paraffin blocks and sectioned for hematoxylin and eosin and IHC at 4-μm thickness. IHC was performed on a Leica bond automated immunostainer (Leica Biosystems) using anti-Ki-67 antibody (Abcam ab16667) at 1:400 dilution. Heat-induced antigen retrieval was conducted using Leica Bond Epitope Retrieval Buffer 2 (EDTA solution, pH 9.0) for 20 minutes. Human prostate adenocarcinoma was used as the positive control. Blocking of nonspecific antibody binding was performed using 5% milk in phosphate buffer saline with Tween 20 (PBS-T). The anti-Ki-67 antibody was detected using Novocastra Bond Refine Polymer Detection and visualized with 3′3-diaminobenzidine (DAB; brown). A hematoxylin nuclear counterstain was applied.

Quantification of the IHC images was performed by manual selection of five regions (anterior right, middle right, posterior, middle left, and anterior left) of the periphery and the core. The periphery was defined as no more than 100 μm from the edge of the tumor excluding the skin, and the core as >1 mm away from the edge of the tumor. An observation window of 100 μm was selected for the core and periphery regions. The percentage of Ki-67 cells was determined from the number of Ki-67 cells normalized to the total number of the cells.

Lactate quantification

Lactate quantification was performed at room temperature with the EnzyChrom L-Lactate Assay Kit (BioAssay Systems) following the manufacturer's protocol. Briefly, the tumor tissue was weighted and homogenized in PBS. The volume of PBS was adjusted to yield the same concentration of tissue in the sample. The sample was then incubated with the working solution of the assay. The optical density of the samples was read out at 560 nm in triplicate and compared with a standard curve at time zero and following a 20-minute incubation. The lactate concentration in the initial tissue was calculated using the recorded weight of the tumor tissue and volume of PBS that was added to the tissue sample.

Bulk gamma counting

4T1 cells (1×10^6) were plated on tissue-culture–treated six-well plates and incubated with RPMI supplemented with either 0, 10, 15, 20, or 25 mmol/L of sodium lactate, lactic acid, or hydrochloric acid ($n = 3$ for each condition). Measurements of the pH of the cell media were performed at 0, 24, and 48 hours using a calibrated Orion pH benchtop meter (ThermoFisher Scientific). At 48 hours, the cells were incubated with glucose-free RPMI media supplemented with FDG (15 MBq/mL) for 30 minutes. The cells were washed 3 times, and their radioactivity was counted using an automated gamma counter (Hidex). Decay correction was applied. Following gamma counting, protein concentration in the sample was determined using a Pierce BCA protein assay kit (ThermoFisher Scientific). Results were expressed in units of counts per minute (CPM) per mg protein. Significance testing (unpaired t test) was perform for all concentrations with respect to the corresponding control.

Results

We explore the role of the tumor microenvironment as a driver of FDG uptake in breast cancer cells using cultured cells and mouse tumor grafts. Both cell lines (mouse 4T1 and human MDA-MB-231 mammary adenocarcinoma) are considered models of late-stage metastatic breast cancer (25). In PET scans and autoradiography, these tumor grafts show reduced FDG signal in the core of the tumor (Fig. 1A–C), a finding also observed in other tumor models (16, 20, 26).

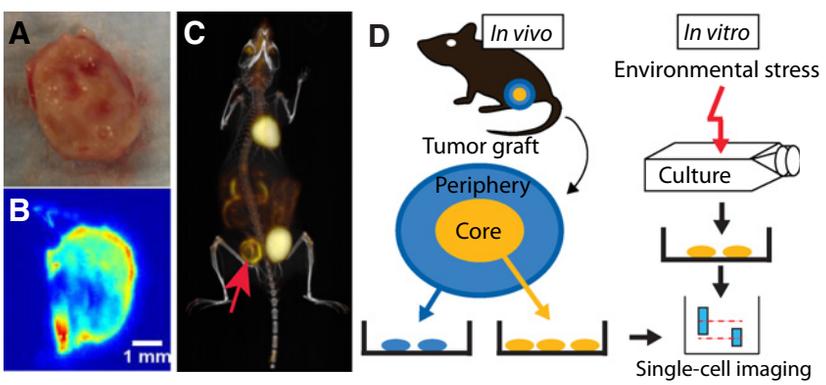

Figure 1.
Heterogeneous FDG uptake in tumor grafts. **A,** Photograph of a 4T1 tumor graft. **B,** Autoradiography of the same tumor shows lower FDG uptake at the center of the tumor compared to the periphery. **C,** PET/CT of mice bearing 4T1 tumor displaying lower uptake of FDG at the core of the tumor (red arrow). **D,** Schematic representation of this study, which aims to measure the effect of the tumor microenvironment on the uptake of FDG by single cells.

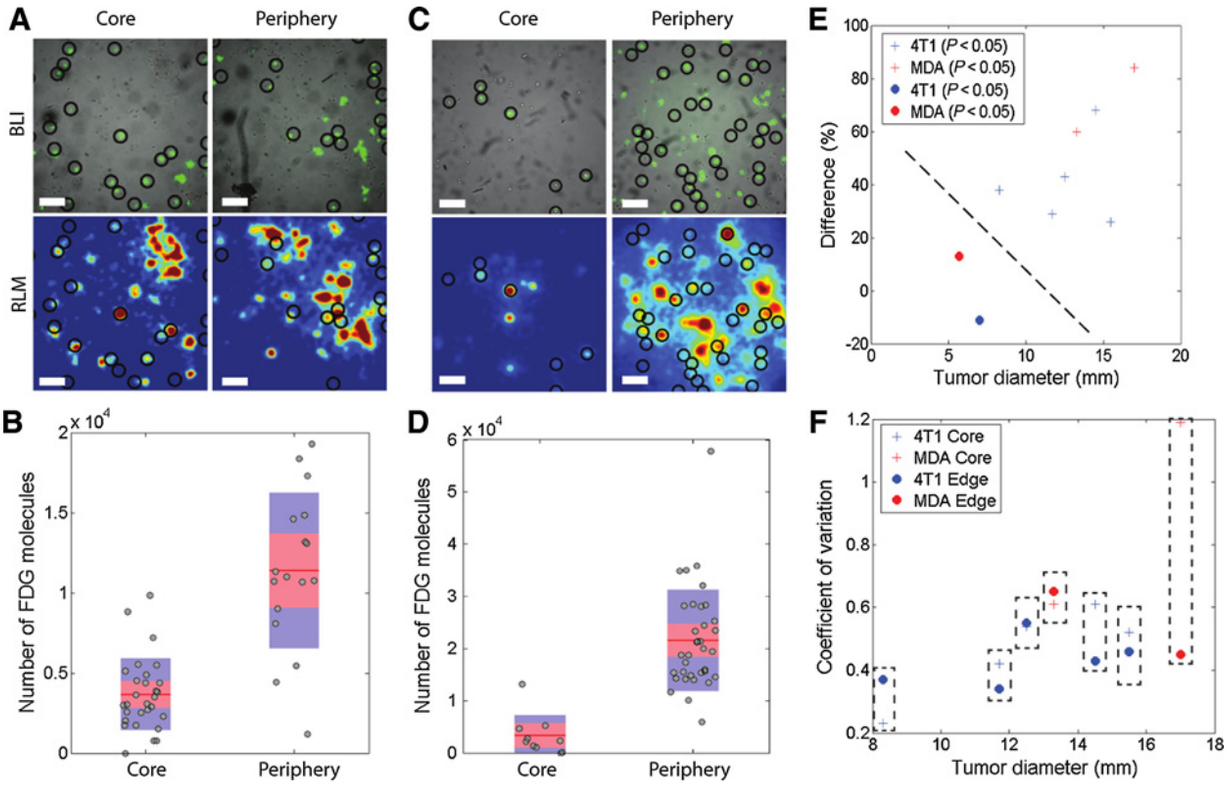

Figure 2.

Single-cell FDG uptake of 4T1 and MDA-MB-231 cells grown as tumor grafts. **A,** Bioluminescence imaging (BLI) and RLM of FDG uptake by cells from core and periphery of a representative 4T1 tumor. Cells selected for analysis are circled in black. **B,** Number of FDG molecules per cell obtained by analyzing the RLM image for single 4T1 cells from core and periphery (gray circles), with mean (red line), SEM (pink rectangle), and 75th percentile (blue rectangle). **C** and **D,** Same for MDA-MB-231 cell line. **E,** Percent difference in mean FDG uptake per cell between tumor core and periphery, as a function of tumor diameter. Blue, 4T1 tumors ($n = 6$); red, MDA-MB-231 ($n = 3$). Statistical difference between core and periphery ($P < 0.05$) is indicated using "+." Other samples are marked as "•." Evidence for a systematic difference between FDG uptake in the core and periphery is strongest for larger tumors. **F,** CV computed from single-cell FDG uptake for the seven tumors larger than 8 mm (i.e., those with significant differences in FDG uptake) in the core (+) and the edge (•) of the tumor in the same animal (dashed box).

To image the heterogeneous FDG uptake of individual cells, we used RLM, a method depicted in Supplementary Fig. S1 and previously described in detail (22). We placed a thin scintillator in contact with the cells of interest to convert radioactive decays from a radiotracer into an optical signal viewable by microscopy. The scintillation signal was recorded by an EM-CCD camera to enable the detection of single radioactive decays at cellular resolution. Live cells were cultured at 10% to 20% confluency on a glass coverslip and exposed to a uniform concentration of FDG. The scintillator was removed for bioluminescence imaging.

RLM of single tumor cells

Tumor specimens were harvested from mice bearing subcutaneous tumor grafts (4T1 and MDA-MB-231 cells) 3 weeks after implantation (Fig. 1D). The tumor was then surgically separated into two components, the periphery and the core. The periphery is characterized by dense, light-colored tissue, whereas the core is markedly softer and darker. Single cells from each dissociated sample were seeded onto glass-bottom dishes for subsequent RLM imaging.

We then used a bioluminescent reporter (Firefly Luciferase) to separate live cancer cells from dead cells and stromal cells. An example of bioluminescence microscopy of cells from a 4T1 tumor graft is shown in Fig. 2A (top row) for cells from the tumor core and periphery. The corresponding FDG uptake, measured using RLM, is shown in Fig. 2A (bottom row). For this specimen, FDG uptake was 68% higher in cells from the periphery than those from the core (Fig. 2B; $P < 10^{-5}$). Another example using the MDA-MB-231 cell line is shown in Fig. 2C and D. For this specimen, the difference in FDG uptake between periphery and core was more pronounced (84%, $P < 10^{-6}$).

A summary of all experiments is provided in Supplementary Table S1. Five of 6 mice bearing 4T1 tumor grafts presented significantly higher FDG uptake per cell in the periphery than in the core, with an average difference of 40% (range, 26%–68%). In the sixth mouse, the difference was below the significance level. For the MDA-MB-231 tumor grafts, the difference between core and periphery was significant in 2 of 3 animals, with an average difference of 72% (range, 60%–84%). Interestingly, we found that statistical significance was achieved in all tumors larger than 8 mm and only in these (Fig. 2E). The difference in FDG uptake was also more prominent for larger tumors.

To rule out the effect of cell seeding density on FDG uptake, we seeded MDA-MB-231 cells at two concentrations and imaged their

FDG uptake with RLM (Supplementary Fig. S2). The seeding conditions did not induce a significant difference in uptake ($P = 0.1$), which is compatible with the results of a previous study (27). We also tested whether differences in single-cell uptake would persist after long-term culture. RLM imaging of cells obtained from tumor grafts shows that core and periphery samples are indistinguishable after 3 weeks in DMEM ($P = 0.9$; Supplementary Fig. S3). For these long-term experiments, the media contained no added lactate and were changed regularly to avoid lactate buildup.

An additional advantage of RLM is that it can measure heterogeneity at the cellular level. Here, we use the coefficient of variation (CV) to measure intrapopulation heterogeneity of FDG uptake. These values are included in Supplementary Table S1 as CV_{Core} and CV_{Peri} for all animals. For animals with significantly heterogeneous microenvironments (i.e., tumors larger than 8 mm), there is a trend toward higher cell-to-cell variability in the core of the tumor than in the periphery (Fig. 2F).

Tumor microenvironment

To elucidate why FDG is taken up differently by cells extracted from the core and periphery of the tumor, we characterized the most salient features of the microenvironment in this tumor model.

Regions of hypoxia are normally defined by their proximity to a connected vasculature. It is commonly observed that the core of a tumor graft is more hypoxic (28, 29). To estimate hypoxia in these animal models, we used qPCR to measure the expression of 84 hypoxia-associated genes in the core and periphery of a 4T1 tumor graft. The assay showed greater than 3-fold upregulation of 15 genes associates with hypoxia signaling, including HIF1 cotranscription factors, apoptosis regulation, metabolism, coagulation, and angiogenesis genes (Fig. 3A; Supplementary Table S2). This finding indicates that, on average, cells in the core of the tumor graft are exposed to a more hypoxic microenvironment than those in the periphery.

Next, we assessed cell proliferation in tumor grafts. First, we measured the incorporation of the thymidine analogue EdU in cells extracted from the core and periphery of tumors. For 4T1 tumors, the fraction of peripheral cells staining positive for EdU was 30% higher than for core cells ($P < 0.04$; Fig. 3B). For MDA-MB-231 tumors, the difference was 7% but not significant (Fig. 3B). To further confirm this effect, we performed IHC staining (Ki-67) of the tumor tissue and found similar results (Fig. 3C and D). Higher Ki-67 staining was observed in the periphery, but the difference was only significant for the 4T1 tumor model (Fig. 3E; $P < 0.03$).

Finally, we measured lactate levels in 4T1 and MDA-MB-231 tumor specimens (Fig. 3F). In the 4T1 tumor model, lactate concentration was significantly higher in the core (22 ± 7 mmol/L) than in the periphery (10 ± 2 mmol/L; $P = 0.02$). The trend was less pronounced for the MDA-MB-231 tumor graft: 17 ± 1 mmol/L for the core and 11 ± 4 mmol/L for the periphery ($P = 0.02$).

In summary, for both tumor graft models, the core of the tumor displayed greater hypoxia, lower proliferation, and higher lactate levels, compared with the periphery. We then sought to replicate these conditions *in vitro* in 4T1 cells to assess whether we could reproduce the observed decrease in the uptake of FDG in the core of the tumor.

Hypoxia (*in vitro*)

Hypoxia is known to render cells more glycolytic through the Pasteur effect, which is mediated by HIF1 activation (30–32). Because FDG uptake is driven by glycolysis, we asked whether hypoxia could explain the pattern of FDG uptake observed in these tumor grafts. We cultured 4T1 cells under normoxia (20% O_2, 7 days) and chronic hypoxia (2% O_2, 7 days) prior to RLM imaging. Mean FDG uptake increased 170% under chronic hypoxia ($P < 10^{-4}$; Fig. 4A; Supplementary Table S3) and, therefore, low FDG uptake in the core of the tumor cannot be explained by chronic hypoxia.

Cell proliferation (*in vitro*)

Growth factors influence glucose metabolism directly (33) and indirectly by inducing cell-cycle arrest in G_0–G_1 (34–36). To study the effect of nutrient availability on FDG uptake, we used RLM to image single 4T1 cells grown in normal (10% FBS) and serum-free (0% FBS) media for 48 hours. FDG uptake data are summarized in Supplementary Table S4 and shown in Fig. 4B. Serum withdrawal decreased FDG uptake by 63% ($P = 0.004$). We also verified that serum withdrawal induced cell-cycle arrest using the EdU assay. The fraction of cells displaying positive EdU fluorescence decreased significantly by 60% after serum was withheld (Supplementary Fig. S4). Together, these data indicate that serum withdrawal arrests cell proliferation and decreases FDG uptake.

Lactic acidosis (*in vitro*)

Finally, we investigate the effect of lactic acid on FDG uptake in 4T1 cells after exposure to 15 mmol/L lactic acid in RPMI 1640 for 48 hours. The medium was changed every 24 hours to stabilize lactic acid concentration. RLM imaging showed that exposure to lactic acid decreased mean FDG uptake by 85% in these cells ($P < 10^{-5}$; Fig. 4C) and increased heterogeneity by 40%, as measured by the CV (Supplementary Table S5).

To further assess the effect of lactic acid, we used gamma counting to measure bulk FDG uptake in 4T1 cells incubated for 48 hours with various concentrations of lactic acid, sodium lactate, and hydrochloric acid (HCl) in RPMI 1640. Extracellular pH was measured for all experiments every 24 hours (Supplementary Table S6; Fig. 4D). FDG uptake was measured in units of CPM and normalized by protein amount per well to account for differences in cell number. For lactic acid, we observe a significant ($P < 0.01$) dose-dependent decrease in FDG uptake (Fig. 4D); the pH of the medium went from neutral (7.4) to moderately acidic (6.9). We then sought to adjust pH independently of lactate ion concentration by titrating HCl. With increasing concentration of HCl, pH went from neutral (7.1) to acidic (6.4), whereas FDG uptake decreased significantly ($P < 0.01$) by up to 80%. Finally, we added equal amounts of lactic acid and sodium hydroxide to titrate lactate ion concentration while keeping pH neutral. (Lactic acid and sodium hydroxide react to yield sodium lactate.) We verified that the medium was neutral (7.0–7.1) at the time of RLM imaging. As with other conditions, lactate ion caused a significant ($P < 0.0001$) dose-dependent decrease in FDG uptake at and above 15 mmol/L, but not for 10 mmol/L. Overall, these data indicate that exposure to acidic pH and lactate ion both inhibits uptake of FDG by 4T1 cells, and thus may explain the observed decrease in FDG uptake seen in tumor grafts.

Discussion

Using RLM, we found significant differences in FDG uptake in populations of single cells derived from the core and periphery of mouse tumor grafts. Because the assay was performed *in vitro* in

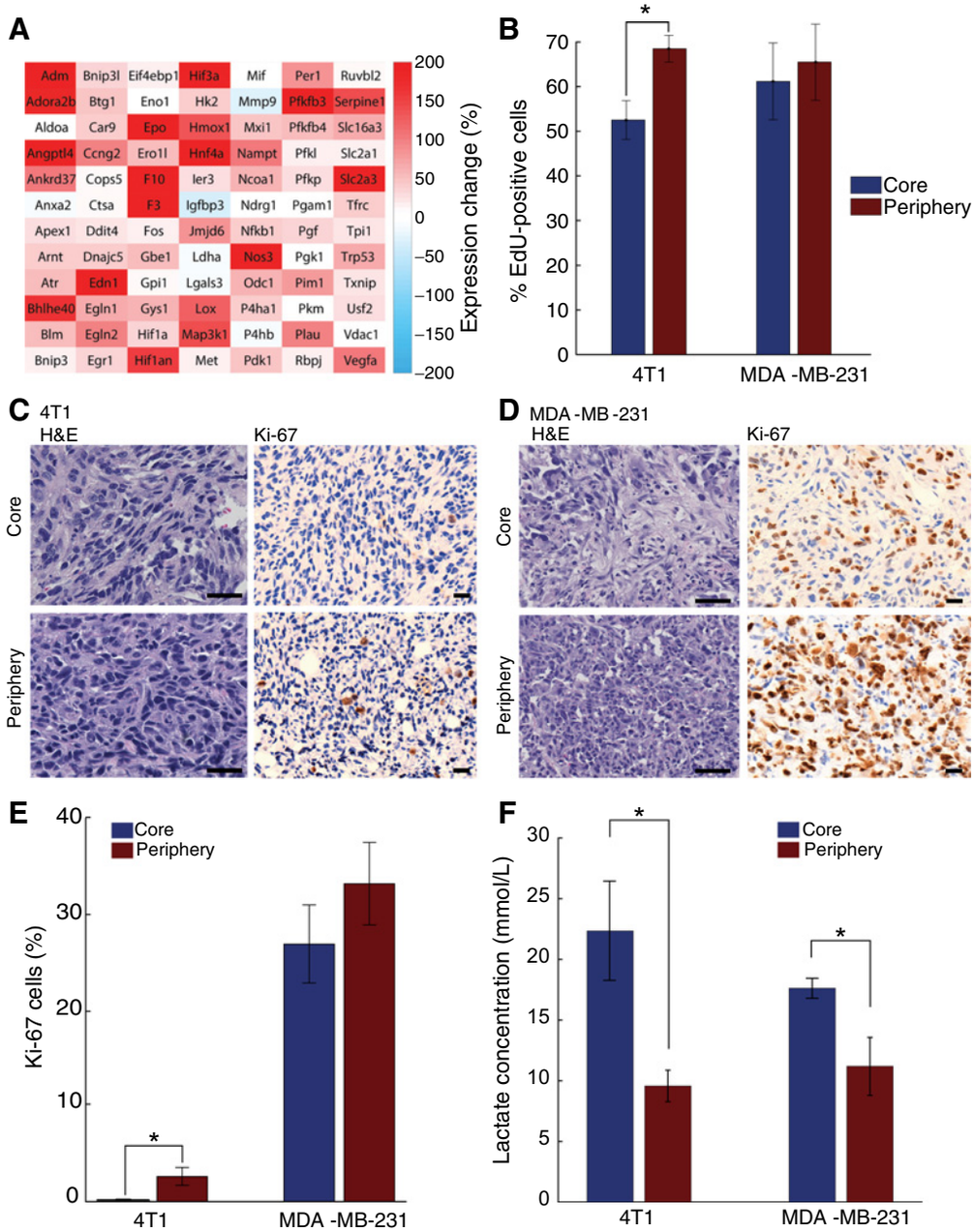

Figure 3.

Microenvironment of tumor grafts. **A,** qPCR analysis of a panel of 84 genes associated with hypoxia. Upregulation (red) of many hypoxia-related genes indicates a more hypoxic environment in the core of the tumor grafts. **B,** Fraction of tumor cells from core and periphery staining positive for EdU incorporation into DNA. **C,** Tumor histology and Ki-67 staining for core and periphery of 4T1 tumor. Scale bars, 50 μm and 20 μm, respectively. **D,** Same for MDA-MB-231 tumor. **E,** Quantitation of the fraction of tumor cells staining positive for Ki-67 for both cell lines shows higher proliferation in the periphery than in the core. **F,** Lactate concentration in the tumor core and periphery for both cell lines. *, $P < 0.05$. H&E, hematoxylin and eosin.

single cancer cells, these differences are inherent to the biology of the tumor cells and not influenced by physical factors such as cell density and radiotracer perfusion. We further examined the effect of three microenvironmental factors on the rate of glycolysis as measured by FDG uptake. Hypoxia is present in the core, but this factor is ruled out as a possible explanation because hypoxia should increase rather than decrease FDG uptake. Next, differences in proliferation between core and periphery were mirrored by differences in FDG uptake, but without evidence of a causal relationship. Finally, lactate was more concentrated in the tumor

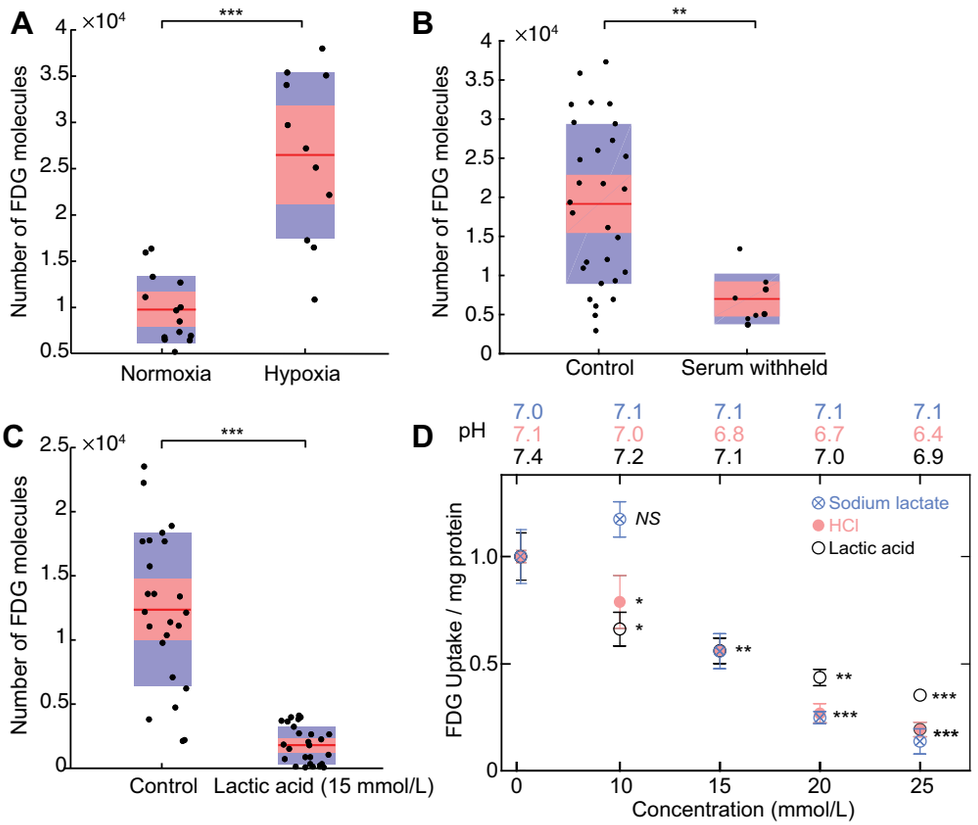

Figure 4.

In vitro FDG uptake for different environmental conditions for 4T1 cells. **A,** Single-cell FDG uptake after 7 days under normoxia or chronic hypoxia (2 % O_2). **B,** Single-cell FDG uptake after 48-hour culture with and without serum. Serum-starved 4T1 cells took up 63% less FDG ($P < 0.005$). Serum removal also caused a decrease in cell proliferation (Supplementary Fig. S4). **C,** Single-cell FDG uptake in 4T1 cells exposed to 15 mmol/L lactic acid for 48 hours. Lactic acidosis caused a decrease in mean FDG uptake of 85% ($P < 10^{-5}$). **D,** Bulk FDG uptake (gamma counting) in cells normalized by protein weight (CPM/mg) as a function of the concentration of sodium lactate (⊗), hydrochloric acid (•), and lactic acid (○). Top, corresponding pH measured prior to incubation with FDG. Significance tests: *NS*, not significant; *, $P < 0.01$; **, $P < 0.001$; ***, $P < 0.0001$.

core, and lactic acid was found to strongly suppress FDG uptake, making lactic acidosis a likely contributor to the observed heterogeneity. The inhibition could be induced by varying pH independently of lactate concentration and, conversely, by varying lactate concentration independently of pH.

This study is motivated by the fact that, clinically, FDG-PET is used to evaluate tumor aggressiveness. PET scans often reveal heterogeneous FDG uptake within tumors, and large tumor masses sometimes display lower FDG uptake in their core (16, 20, 26). Such images are often interpreted to mean that fewer viable cells are present in the center of the tumor. However, our findings suggest that cancer cells in the core of the tumor can also have inherently lower uptake of FDG, as an adaptation to the tumor microenvironment. Cells that grow under conditions of high lactate, low pH, and low oxygen could be as aggressive as those on the periphery of the tumor. In fact, many studies suggest that cells exposed to lactic acidosis have a higher propensity for metastasis. Given the rising interest in using molecular imaging to personalize cancer treatment, it is important to realize that PET scans do not have single-cell resolution and therefore cannot distinguish between a decrease in viable cell density and a decrease in FDG uptake per cell. Single-cell methods such as RLM provide information about FDG uptake by individual cells, albeit in an *in vitro* environment.

Single-cell analysis of the RLM images reveals that cells from the tumor core have significantly lower FDG uptake than those from the periphery (Supplementary Table S1). This was true in 5 of 6 4T1 and in 2 of 3 MDA-MB-231 tumor grafts (Fig. 2). This observation agrees with autoradiography and PET imaging (Fig. 1A–C) and with data from other groups (16, 20, 26). Other xenograft models, however, display higher FDG uptake in the core, which has been attributed to hypoxia (12, 18).

Further analysis showed that the difference in FDG uptake between core and periphery is only significant in larger tumors, namely those greater than 8 mm in diameter (Fig. 2E). This observation has also been made in a PET study with a 4T1 mouse tumor model (37). A minimum tumor volume must be reached for significant different microenvironments to appear and for cancer cells to develop distinct metabolic phenotypes.

The strength of RLM imaging is its single-cell resolution. This technique allows us to isolate cancer cells, check their viability using bioluminescence imaging, and measure their intrapopulation heterogeneity. The level of heterogeneity at the cell level reflects evolutionary pressures that the environment exerts on the

cells. A complex microenvironment where conditions vary rapidly over a small volume will lead to greater cell-to-cell variability, compared with a more uniform environment. A measure of the heterogeneity is the CV, which is defined as the SD of the population divided by the mean. However, for nonnormal distributions, a better metric is the Gini coefficient, a measure developed in economics to quantify income inequality. This measure better captures the stratification in the data and ranges from 0 for equal uptake to 1 for maximal inequality (38). Analysis shows that the mean Gini coefficient for the 4T1 cells is 0.22 ± 0.08 (±0.04) for the original cell line, and 0.29 ± 0.08 (±0.03) for the tumor graft. For the MDA-MB-231 cells, the Gini coefficients for the cell line and tumor graft are 0.18 ± 0.04 (±0.02) and 0.29 ± 0.1 (±0.07), respectively. These numbers indicate that cells extracted from tumor grafts tend to display greater FDG uptake inequality than the original cell line. We attribute this inequality to the action of the tumor microenvironment on the biology of the tumor cells and to the genesis of subpopulations that differ in their glucose metabolism. These clones are not present in normal culture.

Single-cell RLM observations and measurements of microenvironmental factors suggest that hypoxia, acute or chronic, does not play a significant role in driving FDG uptake in these tumor models. Hypoxia is known to render cells more glycolytic through the Pasteur effect, which is mediated by HIF1 activation (30–32). Cells kept under hypoxia (2% O_2 for 7 days) grew slowly but consumed FDG with high avidity (Fig. 4A; Supplementary Fig. S5A). Furthermore, we found evidence of hypoxia in the core of 4T1 tumors, a finding also reported in the MDA-MB-231 tumor xenograft model (39). We conclude that the presence of hypoxia in the core of tumors cannot explain the observed decrease in FDG uptake in that region of the tumor.

In contrast, RLM imaging showed that the rate of FDG uptake in tumor cells mirrored the rate of cell proliferation (Fig. 4B; Supplementary Fig. S5B), confirming previous studies (15, 19). Here, cell proliferation arrest was induced by serum withdrawal, which causes G_0–G_1 cell-cycle arrest. Analysis of the tumor specimens found a higher proliferation at the periphery than at the core (Fig. 3B–E); thus, cell proliferation may explain the observed difference in FDG uptake between the core and edge of the tumor. However, it is unclear that slow proliferation causes cells to decrease their rate of glucose utilization; in fact, cell proliferation and FDG uptake are likely driven by the same microenvironmental factors. A previous study found no change in FDG uptake when the proliferation of HEY *Rab25* cells was modulated by seeding the cells at different densities (27). Furthermore, one effect of serum removal is to cause a decrease in cell metabolism because serum supplies growth factors necessary for PI3K/AKT signaling, a driver of metabolism (40); the decrease in FDG uptake and the arrest of cell proliferation are both consequences of serum withdrawal.

Finally, lactic acidosis appears to be a strong modulator of FDG uptake in this tumor model. Lactate concentration was 2-fold higher in the core than in the periphery of tumor grafts (Fig. 3F). This effect is known to be caused by insufficient removal of waste products due to poor vascularization (41), and it has been observed in human tumor specimens (42, 43). Several studies have reported lactate levels as high as 20 mmol/L in regions of tumors, but it is important to note that *ex vivo* lactate measurements, including those in this study, may overestimate concentration due to anaerobic glycolysis after excision of the tumor.

Elevated levels of lactic acid suppress FDG uptake, as measured with RLM and gamma counting (Fig. 4C and D). Alterations of glycolytic flux by lactic acid have been observed on the cellular level in human monocytes (44, 45) and in tissue (37, 44). Blocking lactate export also inhibits glycolysis by increasing intracellular lactate (46). In cancer, lactic acidosis exerts a negative feedback on glycolysis, forcing cells to switch to oxidative phosphorylation. A detailed study has investigated the role of lactic acidosis on the metabolism of 4T1 cancer cells (47) and made the following important findings: Under lactic acidosis, 4T1 cells switched to an oxidative metabolism, consuming less glucose and producing almost no lactate. The uptake of [^{3}H]2-DG, a molecule biochemically similar to [^{18}F]FDG, was significantly reduced. Although glycolytic enzymes were expressed at similar levels under lactic acidosis, their activity was substantially impaired due to the combined effect of lactate and protons. In addition, lactate can allosterically downregulate the activity of a key glycolytic enzyme, PFK1, by dissociating it into a less-efficient dimer (48). This process is independent of medium acidification. Importantly, these results suggest that HIF-mediated overexpression of glucose transporters and hexokinase enzymes does not necessarily lead to higher FDG uptake because glycolytic enzymes have low activity under acidic conditions or under high lactate concentration. This may explain why we did not observe increased FDG in the hypoxic core of the tumor, despite upregulation of HIF target genes.

Our study confirmed that acidosis is an important factor in the observed decrease in FDG uptake. HCl and lactic acid lead to similar reductions in FDG uptake in 4T1 cells (Fig. 4D), indicating that acidosis is sufficient to inhibit FDG uptake. However, when we evaluated the ability of lactate ion to inhibit FDG uptake, we found that sodium lactate (pH = 7.1 in RPMI) could also downregulate FDG uptake in a dose-dependent manner. We thus conclude that acidosis and lactate ion can both independently inhibit FDG uptake. Furthermore, the effect of combining the two factors (as in lactic acid) was not additive, suggesting that acidosis and lactate ion act on different targets within the glycolytic pathway. It is also important to note that solid tumors have weaker buffering capacity than RPMI, and acidosis could be significant *in vivo* at even lower lactic acid concentrations. Taken together, these data indicate that lactate export by cancer cells and its effect on pH is a likely explanation for the observed decrease their uptake of FDG on the single-cell level.

Fluorescence lifetime microscopy was used in another study to measure the mitochondrial redox state (redox ratio) of MDA-MB-231 xenograft tumors (49). As in the present study, the authors found significant metabolic heterogeneity, with higher oxidation levels in the core of the tumor than in the periphery. They also identified pockets of viable cells inside the necrotic core of the tumor (these may correspond to the cells we imaged from the core of the tumor grafts). These data suggest that, as in our study, cells from the tumor rim have a predominantly glycolytic phenotype (consistent with higher FDG uptake), whereas those from the core rely instead on oxidative metabolism.

Although 4T1 and MDA-MB-231 cells present similar phenotypes in the periphery and the core, there were also differences between the two cell lines. First, differences in cell proliferation between edge and periphery were more significant for the 4T1 cell line (Fig. 3B–E). Second, 4T1 cells (but not MDA-MB-231 cells) upregulated their uptake of FDG when exposed to chronic hypoxia (Fig. 4A; Supplementary Fig. S5A). Third, 4T1 tumors

presented greater disparity in lactate levels between core and periphery (Fig. 3F). Taken together, these findings are consistent with the greater metabolic plasticity of the 4T1 cell line. Compared with other cell lines, the 4T1 cell line has a high capacity for switching between glycolysis and oxidative phosphorylation, resulting in better adaptation to diverse metabolic environments (47, 50).

In summary, our results show that cancer cells reprogram their metabolism to adapt to distinct microenvironments. In these mouse models of breast adenocarcinoma, single cancer cells from the core of the tumor took up less FDG than those from the periphery. Proliferation mirrored FDG uptake but is not thought to be a driving factor. Of all the microenvironmental factors examined, lactic acidosis had the largest impact on FDG uptake. The importance of this finding is that a reduction in FDG uptake in the core of a tumor, which can be measured with a PET scan, could predict elevated lactic acidosis in the tumor. Clinically, elevated lactate levels and acidic pH are an indicator of poor outcome and greater metastatic potential (51, 52). It is also important to consider that FDG uptake, as measured by a PET scan, is not necessarily a measure of the density of viable cells in the tumor, because the microenvironment can alter the intrinsic avidity of individual cells for FDG.

Disclosure of Potential Conflicts of Interest

L.S. Sasportas was a postdoctoral associate at Verily Life Sciences. No potential conflicts of interest were disclosed by the other authors.

Authors' Contributions

Conception and design: S. Türkcan, L. Kiru, L.S. Sasportas, G. Pratx
Development of methodology: S. Türkcan, L. Kiru, G. Pratx
Acquisition of data (provided animals, acquired and managed patients, provided facilities, etc.): S. Türkcan, L. Kiru, D.J. Naczynski, L.S. Sasportas
Analysis and interpretation of data (e.g., statistical analysis, biostatistics, computational analysis): S. Türkcan, L. Kiru, G. Pratx
Writing, review, and/or revision of the manuscript: S. Türkcan, L. Kiru, G. Pratx
Administrative, technical, or material support (i.e., reporting or organizing data, constructing databases): S. Türkcan, L. Kiru
Study supervision: G. Pratx

Acknowledgments

The authors gratefully acknowledge the Stanford Small-Animal Imaging Facility; the Stanford Cyclotron Radiochemistry Facility (Murugesan Subbarayan, George Montoya, and Shawn Scatliffe) for producing and packing ^{18}F-FDG; the Protein and Nucleic Acid Facility; and the author of the NotBoxPlot.m plotting function. This work was supported by a grant from the National Institutes of Health (5R01CA186275 to G. Pratx), a Prostate Cancer Research Program fellowship (W81XWH-14-1-0288 to S. Türkcan), and a postdoctoral training fellowship from the NIH (5T32CA121940 to L. Kiru).

The costs of publication of this article were defrayed in part by the payment of page charges. This article must therefore be hereby marked *advertisement* in accordance with 18 U.S.C. Section 1734 solely to indicate this fact.

Received March 22, 2017; revised April 13, 2018; accepted November 27, 2018; published first December 3, 2018.

References

1. Kostakoglu L, Agress H Jr, Goldsmith SJ. Clinical role of FDG PET in evaluation of cancer patients. Radiographics 2003;23:315–40.
2. Gatenby RA, Gillies RJ. Why do cancers have high aerobic glycolysis? Nat Rev Cancer 2004;4:891–9.
3. Strauss LG. Fluorine-18 deoxyglucose and false-positive results: a major problem in the diagnostics of oncological patients. Eur J Nucl Med Mol Imaging 1996;23:1409–15.
4. Heppner GH. Tumor heterogeneity. Cancer Res 1984;44:2259–65.
5. Marusyk A, Polyak K. Tumor heterogeneity: causes and consequences. BBA Rev Cancer 2010;1805:105–17.
6. Cárdenas-Navia LI, Mace D, Richardson RA, Wilson DF, Shan S, Dewhirst MW. The pervasive presence of fluctuating oxygenation in tumors. Cancer Res 2008;68:5812–9.
7. Graves EE, Maity A, Le Q-T. The tumor microenvironment in non–small-cell lung cancer. Semin Radiat Oncol 2010;20:156–63.
8. Sauer LA, Stayman JW, Dauchy RT. Amino acid, glucose, and lactic acid utilization in vivo by rat tumors. Cancer Res 1982;42:4090–7.
9. Thomlinson R, Gray L. The histological structure of some human lung cancers and the possible implications for radiotherapy. Br J Cancer 1955;9:539.
10. Fukumura D, Jain RK. Tumor microenvironment abnormalities: causes, consequences, and strategies to normalize. J Cell Biochem 2007;101:937–49.
11. Huang T, Civelek AC, Li J, Jiang H, Ng CK, Postel GC, et al. Tumor microenvironment–dependent 18F-FDG, 18F-fluorothymidine, and 18F-misonidazole uptake: a pilot study in mouse models of human non–small cell lung cancer. J Nucl Med 2012;53:1262–8.
12. Pugachev A, Ruan S, Carlin S, Larson SM, Campa J, Ling CC, et al. Dependence of FDG uptake on tumor microenvironment. Int J Radiat Oncol 2005;62:545–53.
13. Aloj L, Caracó C, Jagoda E, Eckelman WC, Neumann RD. Glut-1 and hexokinase expression: relationship with 2-fluoro-2-deoxy-D-glucose uptake in A431 and T47D cells in culture. Cancer Res 1999;59:4709–14.
14. Clavo AC, Brown RS, Wahl RL. Fluorodeoxyglucose uptake in human cancer cell lines is increased by hypoxia. J Nucl Med 1995;36:1625–32.
15. Yamada K, Brink I, Bissé E, Epting T, Engelhardt R. Factors influencing [F18] 2fluoro2deoxyDglucose (F18 FDG) uptake in melanoma cells: the role of proliferation rate, viability, glucose transporter expression and hexokinase activity. J Dermatol 2005;32:316–34.
16. Obata A, Yoshimoto M, Kasamatsu S, Naiki H, Takamatsu S, Kashikura K, et al. Intra-tumoral distribution of 64Cu-ATSM: a comparison study with FDG. Nucl Med Biol 2003;30:529–34.
17. Ong L-C, Jin Y, Song I-C, Yu S, Zhang K, Ong L-C, et al. 2-[18F]-2-deoxy-D-glucose (FDG) uptake in human tumor cells is related to the expression of GLUT-1 and hexokinase II. Acta Radiol 2008;49:1145–53.
18. Zhao S, Kuge Y, Mochizuki T, Takahashi T, Nakada K, Sato M, et al. Biologic correlates of intratumoral heterogeneity in 18F-FDG distribution with regional expression of glucose transporters and hexokinase-II in experimental tumor. J Nucl Med 2005;46:675–82.
19. Avril N, Menzel M, Dose J, Schelling M, Weber W, Jänicke F, et al. Glucose metabolism of breast cancer assessed by 18F-FDG PET: histologic and immunohistochemical tissue analysis. J Nucl Med 2001;42:9–16.
20. Dearling JL, Flynn AA, Sutcliffe-Goulden J, Petrie IA, Boden R, Green AJ, et al. Analysis of the regional uptake of radiolabeled deoxyglucose analogs in human tumor xenografts. J Nucl Med 2004;45:101–7.
21. Pratx G, Chen K, Sun C, Martin L, Carpenter CM, Olcott PD, et al. Radioluminescence microscopy: measuring the heterogeneous uptake of radiotracers in single living cells. PLoS One 2012;7:e46285.
22. Kim TJ, Turkcan S, Pratx G. Modular low-light microscope for imaging cellular bioluminescence and radioluminescence. Nat Protocols 2017;12:1055–76.
23. Sasportas LS, Gambhir SS. Imaging circulating tumor cells in freely moving awake small animals using a miniaturized intravital microscope. PLoS One 2014;9:e86759.
24. Pratx G, Chen K, Sun C, Axente M, Sasportas L, Carpenter C, et al. High-resolution radioluminescence microscopy of 18F-FDG uptake by reconstructing the beta-ionization track. J Nucl Med 2013;54:1841–6.
25. Larive RM, Moriggi G, Menacho-Márquez M, Cañamero M, De Álava E, Alarcón B, et al. Contribution of the R-Ras2 GTP-binding protein to

primary breast tumorigenesis and late-stage metastatic disease. Nat Commun 2014;5:3881.
26. Bao A, Phillips WT, Goins B, McGuff HS, Zheng X, Woolley FR, et al. Setup and characterization of a human head and neck squamous cell carcinoma xenograft model in nude rats. Otolaryngol Head Neck Surg 2006;135:853–7.
27. Witney TH, Carroll L, Alam IS, Chandrashekran A, Nguyen Q-D, Sala R, et al. A novel radiotracer to image glycogen metabolism in tumors by positron emission tomography. Cancer Res 2014;74:1319–28.
28. Maxwell P, Dachs G, Gleadle J, Nicholls L, Harris A, Stratford I, et al. Hypoxia-inducible factor-1 modulates gene expression in solid tumors and influences both angiogenesis and tumor growth. P Natl Aacad Sci U S A 1997;94:8104–9.
29. Serganova I, Doubrovin M, Vider J, Ponomarev V, Soghomonyan S, Beresten T, et al. Molecular imaging of temporal dynamics and spatial heterogeneity of hypoxia-inducible factor-1 signal transduction activity in tumors in living mice. Cancer Res 2004;64:6101–8.
30. Kim J-w, Tchernyshyov I, Semenza GL, Dang CV. HIF-1-mediated expression of pyruvate dehydrogenase kinase: a metabolic switch required for cellular adaptation to hypoxia. Cell Metab 2006;3:177–85.
31. Papandreou I, Cairns RA, Fontana L, Lim AL, Denko NC. HIF-1 mediates adaptation to hypoxia by actively downregulating mitochondrial oxygen consumption. Cell Metab 2006;3:187–97.
32. Seagroves TN, Ryan HE, Lu H, Wouters BG, Knapp M, Thibault P, et al. Transcription factor HIF-1 is a necessary mediator of the Pasteur effect in mammalian cells. Mol Cell Biol 2001;21:3436–44.
33. Vander Heiden MG, Plas DR, Rathmell JC, Fox CJ, Harris MH, Thompson CB. Growth factors can influence cell growth and survival through effects on glucose metabolism. Mol Cell Biol 2001;21:5899–912.
34. Kues W, Anger M, Carnwath J, Paul D, Motlik J, Niemann H. Cell cycle synchronization of porcine fetal fibroblasts: Effects of serum deprivation and reversible cell cycle inhibitors. Biol Reprod 2000; 62:412–9.
35. Miloloza A, Rosner M, Nellist M, Halley D, Bernaschek G, Hengstschläger M. The TSC1 gene product, hamartin, negatively regulates cell proliferation. Hum Mol Gen 2000;9:1721–7.
36. Rosner M, Hengstschläger M. Nucleocytoplasmic localization of p70 S6K1, but not of its isoforms p85 and p31, is regulated by TSC2/mTOR. Oncogene 2011;30:4509.
37. Serganova I, Rizwan A, Ni X, Thakur SB, Vider J, Russell J, et al. Metabolic imaging: a link between lactate dehydrogenase A, lactate, and tumor phenotype. Clin Cancer Res 2011;17:6250–61.
38. Dorfman R. A formula for the Gini coefficient. Rev Econ Stat 1979: 146–9.
39. Quiros-Gonzalez I, Tomaszewski MR, Aitken SJ, Ansel-Bollepalli L, McDuffus L-A, Gill M, et al. Optoacoustics delineates murine breast cancer models displaying angiogenesis and vascular mimicry. Br J Cancer 2018:1.
40. DeBerardinis RJ, Lum JJ, Hatzivassiliou G, Thompson CB. The biology of cancer: metabolic reprogramming fuels cell growth and proliferation. Cell Metab 2008;7:11–20.
41. Vaupel PW, Frinak S, Bicher HI. Heterogeneous oxygen partial pressure and pH distribution in C3H mouse mammary adenocarcinoma. Cancer Res 1981;41:2008–13.
42. Kennedy KM, Scarbrough PM, Ribeiro A, Richardson R, Yuan H, Sonveaux P, et al. Catabolism of exogenous lactate reveals it as a legitimate metabolic substrate in breast cancer. PLoS One 2013;8:e75154.
43. Walenta S, Schroeder T, Lehr H-A, Kunz-Schughart LA, Fuerst A, Mueller-Klieser W. Metabolic classification of human rectal adenocarcinomas: a novel guideline for clinical oncologists? J Cancer Res Clin Oncol 2003; 129:321–6.
44. Busk M, Walenta S, Mueller-Klieser W, Steiniche T, Jakobsen S, Horsman MR, et al. Inhibition of tumor lactate oxidation: consequences for the tumor microenvironment. Radiother Oncol 2011;99:404–11.
45. Dietl K, Renner K, Dettmer K, Timischl B, Eberhart K, Dorn C, et al. Lactic acid and acidification inhibit TNF secretion and glycolysis of human monocytes. J Immunol 2010;184:1200–9.
46. Doherty JR, Yang C, Scott KE, Cameron MD, Fallahi M, Li W, et al. Blocking lactate export by inhibiting the Myc target MCT1 Disables glycolysis and glutathione synthesis. Cancer Res 2014;74:908–20.
47. Xie J, Wu H, Dai C, Pan Q, Ding Z, Hu D, et al. Beyond Warburg effect–dual metabolic nature of cancer cells. Sci Rep 2014;4:4927.
48. Leite TC, Da Silva D, Coelho RG, Zancan P, Sola-Penna M. Lactate favours the dissociation of skeletal muscle 6-phosphofructo-1-kinase tetramers down-regulating the enzyme and muscle glycolysis. Biochem J 2007; 408:123–30.
49. Xu HN, Nioka S, Glickson JD, Chance B, Li LZ. Quantitative mitochondrial redox imaging of breast cancer metastatic potential. J Biomed Opt 2010;15:036010.
50. Simões RV, Serganova IS, Kruchevsky N, Leftin A, Shestov AA, Thaler HT, et al. Metabolic plasticity of metastatic breast cancer cells: adaptation to changes in the microenvironment. Neoplasia 2015;17:671–84.
51. Martinez-Outschoorn UE, Prisco M, Ertel A, Tsirigos A, Lin Z, Pavlides S, et al. Ketones and lactate increase cancer cell "stemness," driving recurrence, metastasis and poor clinical outcome in breast cancer: achieving personalized medicine via Metabolo-Genomics. Cell Cycle 2011;10:1271–86.
52. Walenta S, Schroeder T, Mueller-Klieser W. Lactate in solid malignant tumors: potential basis of a metabolic classification in clinical oncology. Curr Med Chem 2004;11:2195–204.